HAL
open science

# A search for low surface brightness dwarf galaxies in different environments

Sarah Roberts, Jonathan Davies, Sabina Sabatini, Willem van Driel, Karen L. O'Neil, Maarten Baes, Suzanne Linder, Rodney Smith, Rhodri Evans

## To cite this version:

Sarah Roberts, Jonathan Davies, Sabina Sabatini, Willem van Driel, Karen L. O'Neil, et al.. A search for low surface brightness dwarf galaxies in different environments. Monthly Notices of the Royal Astronomical Society, 2004, 352, pp.478-492. 10.1111/j.1365-2966.2004.07934.x . hal-03742546

**HAL Id: hal-03742546**

**https://hal.science/hal-03742546v1**

Submitted on 23 Feb 2023

**HAL** is a multi-disciplinary open access archive for the deposit and dissemination of scientific research documents, whether they are published or not. The documents may come from teaching and research institutions in France or abroad, or from public or private research centers.

L'archive ouverte pluridisciplinaire **HAL**, est destinée au dépôt et à la diffusion de documents scientifiques de niveau recherche, publiés ou non, émanant des établissements d'enseignement et de recherche français ou étrangers, des laboratoires publics ou privés.

Mon. Not. R. Astron. Soc. **352,** 478–492 (2004) doi:10.1111/j.1365-2966.2004.07934.x

# A search for low surface brightness dwarf galaxies in different environments

Sarah Roberts,[1★] Jonathan Davies,[1] Sabina Sabatini,[1] Wim van Driel,[3] Karen O'Neil,[4] Maarten Baes,[1,2] Suzanne Linder,[1] Rodney Smith[1] and Rhodri Evans[1]

[1]*School of Physics and Astronomy, Cardiff University, PO Box 913, Cardiff CF24 3YB*
[2]*Sterrenkundig Observatorium, Gent University, Belgium*
[3]*Observatoire de Paris, GEPI, 5 Place Jules Janssen, 92195, Meudon, France*
[4]*NRAO, Green Bank Telescope, PO Box 2, Rt. 28/29, Green Bank, WV 24944-0002, USA*

Accepted 2004 April 21. Received 2004 April 20; in original form 2003 September 15

## ABSTRACT

According to the cold dark matter (CDM) hierarchical clustering theory of galaxy and large-scale structure formation, there should be numerous low-mass dark matter haloes present in the Universe today. If these haloes contain sufficient stars, they should be detectable as low-luminosity stellar systems or dwarf galaxies. We have previously described a new detection method for faint low surface brightness objects and we have shown that there are relatively large numbers of very faint dwarf galaxies in the nearby Virgo cluster. In this paper, we present results from a similar survey carried out on the Millennium Galaxy strip, which runs along the celestial equator and samples a very different galaxy environment. We show that the dwarf-to-giant galaxy number ratio along this strip ranges from 0.7 : 1 to, at most, 6 : 1, corresponding to a flat luminosity function ($\alpha \approx -0.8$ to $-1.0$). This is very different to our value of 20 : 1 for the Virgo cluster. There is no population of low surface brightness dwarf galaxies in the field that have gone undetected by the redshift surveys. This result is exactly opposite to what CDM models predict for the environmental dependence of the dark matter mass function, which is that there are proportionally more small dark matter haloes in lower-density environments.

**Key words:** surveys – galaxies: clusters: individual: Virgo cluster – galaxies: clusters: individual: Ursa Major – galaxies: dwarf.

## 1 INTRODUCTION

Data from the recent large redshift surveys carried out by Sloan and 2dF have been used to define the global (averaged over all environments) luminosity function (LF) of galaxies (Blanton et al. 2001; Norberg et al. 2002). These two surveys produce a consistent result for the faint-end slope of the LF, $\alpha \approx -1.2$. This value is somewhat flatter than typically predicted by most cold dark matter (CDM) models of large-scale structure and galaxy formation unless some form of dwarf galaxy formation suppression is invoked (Cole et al. 2000; Mathis et al. 2002). A challenge for the numerical modellers is the observed environmental dependence of the relative dwarf galaxy numbers discussed in this paper.

Dwarf galaxies have been found in large numbers in a variety of rich, high-density environments: Virgo cluster (Binggeli, Sandage & Tarenghi 1984); Coma cluster (Milne & Pritchet 2002); Fornax cluster (Kambas et al. 2000). However, the evidence is growing that the large number of dwarfs predicted by standard CDM theory[1] [mass (luminosity?) function faint-end slope $\alpha \approx -2$] fail to appear in lower-density environments. According to the standard CDM model, dwarf galaxies form when initial Gaussian density fluctuations in the primeval Universe grow linearly, collapse and virialize to produce what we see as dwarf galaxies. Simulations and semi-analytical models have been looked at to see what predictions CDM theory makes about the local dwarf galaxy population. For example, Kauffmann, White & Guideroni (1993) used semi-analytical models to look at the formation of galaxies within this hierarchical clustering theory (see also Cole et al. 2000; Mathis et al. 2002). Using a standard CDM model, they looked at both a dark matter halo with a circular velocity, $V_{\rm circ} \approx 200$ km s$^{-1}$, comparing its LF to observations of the Milky Way (MW), and also a dark matter halo with $V_{\rm circ} \approx 1000$ km s$^{-1}$, comparing this LF to observations of the Virgo cluster. From their model of the MW sized halo, their calculations predicted 5–10 times more faint, low-mass galaxies than

★E-mail: sarah.roberts@astro.cf.ac.uk

[1] By standard CDM we mean a model that does not invoke dwarf galaxy suppression mechanisms, as discussed later in this introduction.

© 2004 RAS

Downloaded from https://academic.oup.com/mnras/article/352/2/478/1011536 by guest on 23 February 2023

observation showed. Moore et al. (1999a) have also conducted numerical simulations of CDM hierarchical galaxy formation to compare predictions with observations of the MW and Virgo cluster. The circular velocity (mass) distribution of the haloes they simulated for both the MW and Virgo cluster were very similar, differing only by the scaling factor of the halo mass, although the cluster halo was 2500 times larger than the galaxy halo and formed 5 Gyr later. They found that their simulations agreed well with Virgo cluster observations – a plot of the abundance of haloes as a function of their circular velocity showed that the simulated and observed Virgo cluster numbers were very similar. However, the simulated galaxy haloes, when compared to that of the Local Group (LG) dwarf galaxies, overpredicted the total number of satellites larger than dwarf spheroidals (dSphs) by a factor of about 50 (see also Klypin et al. 1999).

Although the above papers highlight the discrepancy between simulation and observation, we should be careful with this comparison. In the main, the simulations are of dark matter haloes and it is these that are overproduced in the simulations. To relate dark matter haloes to observations of luminous galaxies requires some modelling of the way in which baryonic material falls into the dark halo and how it is subsequently converted into stars. These physical processes are not so straightforward to model as those used in a standard CDM simulation. Attempts to make the observations and predictions match up include suppressing the formation of dwarf galaxies with a photoionizing background (Efstathiou 1992; Dijkstra et al. 2004), inhibiting star formation by expelling gas, a 'feedback' mechanism (Dekel & Silk 1986) and merging the fainter galaxies so their number decreases. Kauffmann et al. (1993) concluded that it was very difficult to suppress the formation of so many dwarf galaxies compared to observation – this is often referred to as the substructure problem. Other possible solutions to the substructure problem that do not fit so well within the standard CDM model are that the initial power spectrum is wrong (Kamionkowski & Liddle 2000), that baryonic material does not fall into small haloes – they remain dark (Bullock, Kravtsov & Weinberg 2000), that baryonic material falls in, but fails to form stars or stars do form, however there are so few they have so far failed to be detected. It is the last of these solutions that we intend to investigate as part of the work described in this paper. Our motivation is that recent determinations of the field galaxy LF (for example 2dF, see Norberg et al. 2002) have relied upon data obtained from photographic plates that are only sensitive to relatively high surface brightness objects (isophotal limit of $\approx$24.5 $B\mu$). In the LG and in nearby clusters there is a well-defined surface brightness magnitude relation (Ferguson & Binggeli 1994) such that low-luminosity objects also have low surface brightness (LSB) – they are doubly cursed. Photographic surveys would miss many of these faint LSB dwarf galaxies and, even if detected, it is then very difficult to obtain redshifts, even with the largest telescopes. Thus, potentially there may be many dwarf galaxies missing, due to selection effects, from the data used to derive the LF. This issue has also been discussed extensively by Cross et al. (2001), Cross & Driver (2002) and Liske et al. (2003). What we bring new to this discussion is a detection algorithm that is optimized to find LSB dwarf galaxies and a direct comparison with surveys sampling the galaxy population in different environments. So, our second motivation is that there appears to be a strong environmental affect on the relative numbers of dwarf compared to giant galaxies. How can CDM and its associated dwarf galaxy formation suppression mechanisms explain this?

A further important point is that the large redshift surveys have only accurately measured the LF for $M_B < -17$ (Driver & de Propis 2003). It is not at all clear whether the extrapolation of the LF to fainter magnitudes is valid. The only environment where the LF appears to be well measured fainter than $M_B = -17$ is the LG (Mateo 1998; Pritchet & van den Bergh 1999) and this gives a flat faint-end slope ($\alpha = -1.1$) down to the faint magnitudes ($M_B = -10$) we explore in this paper.

Various other surveys have previously been carried out to quantify the population of dwarf galaxies in different environments (Trentham 1997; Chiboucas & Mateo 2001; Trentham & Hodgkin 2002). These studies usually take the form of finding the faint-end slope of the LF (described by a Schechter function) for a sample of galaxies in some field, group or cluster environment. Comparing surveys is very difficult because they are often in different bands and have different magnitude and surface brightness limits. For example, Trentham & Tully (2002) find the $B$-band faint-end slope of the LF of the Virgo cluster to be $\approx -1.4$ for galaxies fainter than $M_B = -18$, and compare it to the value obtained by Phillipps et al. (1998) who found a steeper value of $-2.2$ in the $R$-band, using a very different method to identify cluster galaxies. In their paper, Trentham & Hodgkin also comment on the shallow LF obtained for the Ursa Major (UMa) cluster (Trentham, Tully & Verheijen 2001), but their data for the two clusters was obtained using different instruments and different filters. The method of selecting galaxies is also carried out in different ways for different surveys. Of particular concern is deciding which galaxies are cluster members and which are background, redshifts being difficult to obtain for faint LSB objects. In their study of the UMa cluster, Trentham et al. (2001) find a condition for membership of the cluster based on measured light concentrations of the galaxies. They use the magnitude versus central surface brightness relation of Ferguson & Binggeli (1994) and say that, for a given apparent magnitude, the concentration of light for cluster dwarf galaxies will be less concentrated than for background galaxies of the same apparent magnitude due to the dwarf's lower surface brightness and larger sizes. Trentham et al. state, that any dwarf galaxies which satisfy both these criteria are possible cluster members, although there is some contamination from background objects (see their paper for further details). They give no independent demonstration that their selection method works. Phillipps et al. (1998) use an entirely different method. They subtract galaxy counts obtained from fields outside the cluster away from those inside the cluster to be left with the residual (small) cluster contribution. These methods have consistently led to LFs much steeper than those derived by other methods. It is not difficult to see why – the 'clumpiness' of the background and the subtraction of one large number from another to leave a small residual. If the background count slope is 0.6 m and this remains in the residual, then the inferred LF faint-end slope would be a very steep $-2.5$ (see also Valotto, Moore & Lambas 2001). In our previous work (Sabatini et al. 2003) we demonstrate (decreasing number density with distance from the cluster centre) that with the correct selection criteria we are able to preferentially select cluster dwarf galaxies.

To be able to make proper comparisons of the LFs in different environments, all variables (e.g instrument, band, exposure times, selection criteria) should ideally be the same. This is what we have tried to do with the three 'environments' described in this paper. Our three surveys were conducted using the same instrument, technique (filter band, exposure time) and selection criteria. We can be confident therefore that, unlike similar studies, we are comparing 'like with like'. Throughout this paper we use $H_0 = 75$ km s$^{-1}$ Mpc$^{-1}$.

Downloaded from https://academic.oup.com/mnras/article/352/2/478/1011536 by guest on 23 February 2023

## 2 DATA

### 2.1 The instrument

The optical data for this paper were obtained using the Wide Field Camera (WFC) on the Isaac Newton Telescope, La Palma, Canary Islands as part of the Wide Field Survey, a multicolour data survey covering over 200 deg$^2$ of sky. The WFC is a mosaic of four thinned EEV 4K × 2K CCDs with a pixel size of 0.33 arcsec and total sky coverage of 0.29 deg$^2$. Images on CCD 3 were not used due to its vignetting so our total field of view was 0.21 deg$^2$. All images were taken in the *B*-band for 750 s. All data reduction was carried out by the Cambridge Astronomical Survey Unit pipeline (http://www.ast.cam.ac.uk/∼wfcsur/index.php). This included de-biasing, bad pixel replacement, non-linearity correction, flat-fielding, de-fringing and gain correction.

For the photometry of the objects, colours were obtained from the Sloan Digital Sky Survey (SDSS) website.

### 2.2 The data sets

#### 2.2.1 *Millennium Galaxy strip*

The Millennium Galaxy strip (MGS) data were obtained during four observing runs in 1999 and 2000 and consist of 144 fields running along the celestial equator (full details can be found in Liske et al. 2003). The first field was positioned at $\alpha$ (J2000) $=10^{\rm h}00^{\rm m}00^{\rm s}$, $\delta$ (J2000) $= 00^\circ00'00''$, with the following fields offset by 30 arcmin along the equator. The final field was therefore at $\alpha$ (J2000) $= 14^{\rm h}48^{\rm m}00^{\rm s}$, $\delta$ (J2000) $= 00^\circ00'00''$. The total area used is 30 deg$^2$ and extends through local regions of high and low galactic density. The strip begins in the Leo group, passing very close to NGC 3521, before running through a relatively empty local area of space. The strip then passes through the Virgo Southern Extension, and back into a lower-density region on the other side of the extension before ending in the higher-density Virgo III cloud. Fig. 1 illustrates the position of the data strip in relation to all galaxies listed in the NASA/IPAC Extragalactic Database (NED) within 4500 km s$^{-1}$. The Virgo Southern Extension can be seen at approximately the middle of the data strip. Although called the Virgo Southern Extension, it is not actually part of the Virgo cluster itself. de Vaucouleurs (1961) stated that 'the southern Virgo cloud is closely similar to the UMa cloud and probably no more directly related to the Virgo cluster proper, except in so far as both are galaxy clouds within the Local Supercluster'. The galaxies in this region therefore are not necessarily cluster galaxies, and could be field objects. The MGS passes through regions both rich and devoid of local bright galaxies, so it is an excellent data set for a study of the influence of the environment on populations of dwarf galaxies.

#### 2.2.2 *Virgo cluster*

The Virgo cluster is an irregularly shaped, dense cluster of galaxies situated at a distance of approximately 16 Mpc (Jerjen et al. 2004), $v_{\rm M87} \approx 1300$ km s$^{-1}$. Containing several hundred giant galaxies and a large population of dwarf galaxies (Binggeli et al. 1984), it is an ideal place to look for an environmental dependence of the LF compared to the less rich environment sampled by the MGS data. The cluster has a crossing time of approximately $0.1H_0$ (Trentham & Hodgkin 2002) and so is a dynamically evolved cluster with a high probability of many galaxy interactions having occurred. It is also an X-ray cluster and so in the cluster core galaxies move through a hot intergalactic gas (Young, Wilson & Mundell 2002). In addition, being one of the closest clusters to ourselves, Virgo is also one of the most observed, so there is a wealth of data with which results can be compared. The Virgo cluster survey carried out by Sabatini et al. (2003) consisted of imaging two perpendicular strips extending outwards from the cluster centre (defined as M87) for 7 and 5 degrees (see Fig. 1). The total area covered in the survey was ≈25 deg$^2$. The results for the east–west strip, with which we shall be comparing our results, are presented in Sabatini et al. (2003).

#### 2.2.3 *Ursa Major cluster*

The UMa cluster is a loose irregular cluster of predominantly spiral-type galaxies at approximately the same distance ($v \approx 900$ km s$^{-1}$)

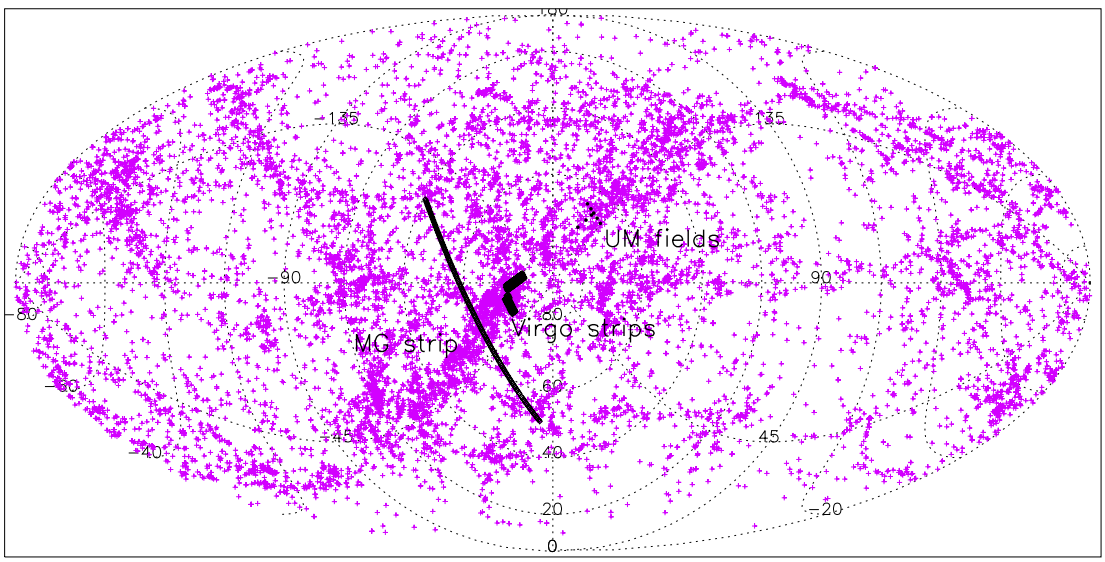


**Figure 1.** Positions of MGS, Virgo cluster data strips and fields in UMa viewed from the North Galactic Pole. The MGS is indicated by the long thin line, which passes through the Virgo Southern Extension at approximately its mid-point. The two Virgo data strips are situated above the MGS, whilst the UMa fields can be seen plotted as filled circles. Also plotted are all galaxies listed in the NED with $v < 4500$ km s$^{-1}$.



Downloaded from https://academic.oup.com/mnras/article/352/2/478/1011536 by guest on 23 February 2023

as Virgo (Trentham & Hodgkin 2002). It has a dynamical crossing time which is comparable to a Hubble time (Trentham & Hodgkin 2002), therefore is dynamically un-evolved with few galaxy–galaxy interactions having occurred. Such a cluster is interesting to study and compare with a more dynamically evolved cluster such as Virgo. Our data fields, obtained in the spring of 2002, are shown in Fig. 1 in relation to the other data sets for the MGS and the Virgo cluster. The circles in Fig. 1 represent the positions of our fields varying with distance from the cluster centre. A total of eight fields covering 1.68 deg$^2$ were obtained using the same instrumental set-up and exposure times as the MGS and Virgo cluster surveys. The fields that we chose correspond to some of the fields looked at by Trentham et al. (2001), although their total area was slightly larger at 2.2 deg$^2$.

### 2.3 H I follow-up observations

One of the greatest limitations to understanding the number density of dwarf galaxies has been the difficulty of obtaining distances (see, for example, Jerjen et al. 2001). There are two reasons for this. The first, as described in the introduction, is that many dwarf galaxies have very low surface brightness. This makes it extremely difficult to obtain an optical redshift. The second reason is that many dwarf galaxies (particularly in clusters) are apparently devoid of atomic gas, making a 21-cm redshift impossible also. We have obtained, from the Millennium Galaxy Catalogue (Driver, private communication), a number of optical redshifts for our detections, listed as $v_{\rm opt}$ in Table 1. Given that field dwarf galaxies tend to be gas-rich compared to cluster dwarfs (Sabatini et al. 2003) we have also obtained 21-cm data for a number of our detections (listed as $v_{\rm H\,I}$ in Table 1).

The 305-m Arecibo telescope was initially used to observe a pilot sample of 12 objects from our catalogue of candidate LSB dwarf galaxies in 2003 May and a further 56 objects were observed in 2004 January. Data were taken in 2003 with the *L*-band narrow receiver (see Sabatini et al. 2003) and in 2004 with the *L*-band wide receiver, in both cases using nine-level sampling with two of the 2048 lag subcorrelators set to each polarization channel. All observations were taken using the position-switching technique, with the blank sky (or OFF) observation taken for the same length of time, and over the same portion of the Arecibo dish as was used for the on-source (ON) observation. Each 5min + 5min ON + OFF pair was followed by a 10-s ON + OFF observation of a well-calibrated noise diode. The overlaps between both subcorrelators with the same polarization allowed a wide velocity search while ensuring an adequate coverage in velocity. The velocity search range was 100–9600 km s$^{-1}$ and the velocity resolution was 2.6 km s$^{-1}$. The instrument's half power beamwidth at 21 cm was 3.6 arcmin and the pointing accuracy was about 15 arcsec. The pointing positions used were the optical centre positions of the target galaxies listed in Tables 1 and 2.

Using standard IDL data reduction software available at Arecibo, corrections were applied for the variations in the gain and system temperature with zenith angle and azimuth, a baseline of order one to three was fitted to the data, excluding those velocity ranges with H I line emission or radio frequency interference (RFI), the velocities were corrected to the heliocentric system, using the optical convention, and the polarizations were averaged. All data were boxcar smoothed to a velocity resolution of 12.9 km s$^{-1}$ for further analysis. For all spectra, the rms noise level was determined and, for the detected lines, the central velocity, velocity width at the 50 per cent level of peak maximum and the integrated flux were determined. Tables 1 and 3 list those galaxies detected at 21 cm.

Given a typical rms noise of 0.6 mJy in our smoothed spectra, we expect to be able to detect a dwarf galaxy with a velocity width of 75 km s$^{-1}$ and $M_{\rm H\,I} \approx 10^7$ M$_\odot$ at a distance of 21 Mpc (see below). This leads to a minimum $M_{\rm H\,I}/L_B$ of 0.24 for the brightest galaxy in our sample ($M_B = -14$) and $M_{\rm H\,I}/L_B$ almost equal to 10 for an $M_B = -10$ galaxy. Given these large values of $M_{\rm H\,I}/L_B$ it is not possible to use the non-detection of H I as an indication that these objects lie at large redshifts. In order to identify sources whose H I detections might have been confused by nearby galaxies, we queried the NED and the HyperLeda data base and inspected DSS images over a region of 10-arcmin radius surrounding the centre position of each source.

## 3 OPTICAL DETECTION ALGORITHM

LSB objects are difficult to detect as their surface brightnesses are below that of the sky ($\approx 23 B\mu$). Standard detection algorithms, for example SEXTRACTOR (Bertin & Arnouts 1996), use the 'connected pixels' method to find objects; a group of connected pixels that are above a threshold value from the background is identified as a detection. However, as this only makes use of the connected pixels, the signal-to-noise ratio for the detection is high, thus low signal-to-noise LSB galaxies are selected against. The algorithm implemented in this project was developed with the specific aim of emphasizing faint, diffuse objects on CCD frames, i.e to detect LSB objects. The method uses a Fourier convolution with matched templates and is fully explained in Sabatini et al. (1999, 2003); the main steps are outlined below.

(i) Background fluctuation flattening is carried out using SEXTRACTOR and gives a homogeneous flat image. SEXTRACTOR divides the image into a grid of subarrays (which are large compared to the object size) and estimates a value for the local sky from this grid. Any values over $3\sigma$ from the median of this value are then removed. This only reduces the noise by about 6 per cent but improves the use of filters later on in the detection process.

(ii) To minimize any contamination of the sample, the removal of other astronomical objects, e.g stars, bright galaxies, etc., must be carried out prior to convolution of the image with the filters. There are two parts to this process: first, the big bright objects must be removed, followed by the small, sharp objects. It would be possible to use SEXTRACTOR for this purpose, but as it is not very efficient and leaves stellar haloes in the final image, a separate program was written for the purpose of removing saturated and bright objects. SEXTRACTOR is then used for the smaller stellar objects. The program removes the bright objects by masking the region with the median sky value plus its Poissonian noise. As this could also result in galaxies being removed from the image if their centres were on the border of the mask, simulations were carried out to check at what distance a galaxy could be from a masked region before it was also removed.

(iii) The convolution of the image is performed using specifically designed filters. The first problem when looking at designing a filter is what size to choose for detection of LSB galaxies. As galaxies come in different sizes, so too should the filters. This would result in having to use a very wide bandpass filter, which would then give many unwanted objects. Using different filters of each size and looking at the results from each would take a long time to do. It was decided that the best option was to apply a combination of filters of different sizes, which would give a final significance image with each different size being emphasized at the same time. This image can then be used as a map of the positions of the candidates.



Downloaded from https://academic.oup.com/mnras/article/352/2/478/1011536 by guest on 23 February 2023

**Table 1.** Table of sure optical detections in the MGS. In the comments column, NO and ND denote 'not observed' and 'observed but not detected' at 21 cm, respectively. Note that objects 10/11 and 12/13 lie in the same Arecibo beam, but are distinct in the optical image (see text). Objects 34 and 42 are possible detections and will need confirming.

| Index | RA (J2000) ($^{h\ m\ s}$) | Dec. (J2000) ($^{\circ\ \prime\ \prime}$) | $m_B$ | $\mu_0$ | Scalelength (arcsec) | Comments | $\log M_{\rm H\,I}$ ($M_\odot$) | $W_{50}$ (km s$^{-1}$) | Velocity (km s$^{-1}$) |
|---|---|---|---|---|---|---|---|---|---|
| 1 | 10 10 42.01 | −0 07 39.6 | 17.7 | 23.2 | 5.0 | Spiral, NO | – | – | $v_{\rm opt} = 17,630$ |
| 2 | 10 12 32.73 | −0 09 45.3 | 18.1 | 23.1 | 4.0 | Irr, NO | – | – | $v_{\rm opt} = 17,214$ |
| 3 | 10 22 20.79 | −0 15 51.3 | 20.0 | 25.0 | 4.0 | Irr, ND | – | – | – |
| 4 | 10 29 23.30 | −0 16 05.0 | 19.4 | 24.9 | 5.0 | ? | 8.9 | 44 | $v_{\rm H\,i} = 7323$ |
| 5 | 10 35 29.38 | −0 00 54.7 | 17.1 | 23.3 | 7.0 | Irr, NO | – | – | $v_{\rm opt} = 8400$ |
| 6 | 10 40 14.92 | −0 06 46.2 | 19.1 | 24.1 | 4.0 | Irr | 8.7 | 117 | $v_{\rm H\,I} = 5642$ |
| 7 | 10 39 34.40 | −0 08 49.9 | 25.2 | 20.2 | 4.0 | Spheroidal, ND | – | – | – |
| 8 | 10 39 23.75 | −0 16 45.4 | 19.6 | 25.5 | 6.0 | ?, ND | – | – | |
| 9 | 10 44 43.56 | −0 11 39.6 | 16.9 | 23.1 | 7.0 | Irr, NO | – | – | $v_{\rm opt} = 4479$ |
| 10 | 10 52 40.55 | −0 01 15.9 | 18.2 | 23.2 | 4.0 | Irr | 8.1 | 69 | $v_{\rm H\,I} = 1772$ |
| 11 | 10 52 39.61 | −0 00 36.9 | 20.7 | 25.7 | 4.0 | Sph | – | – | – |
| 12 | 11 04 40.22 | 0 03 29.5 | 16.9 | 23.7 | 9.0 | Spheroidal | 6.2 | 25 | $v_{\rm H\,I} = 835$, $v_{\rm opt} = 801$ |
| 13 | 11 04 38.60 | 0 04 53.8 | 20.2 | 25.2 | 4.0 | Spheroidal | – | – | – |
| 14 | 11 04 20.55 | 0 01 18.4 | 19.6 | 24.6 | 4.0 | Irr, ND | – | – | – |
| 15 | 11 12 50.23 | 0 03 37.1 | 18.0 | 23.0 | 4.0 | Spheroidal, NO | – | – | $v_{\rm opt} = 28,636$ |
| 16 | 11 15 26.76 | −0 09 40.9 | 18.3 | 23.2 | 4.0 | Spiral, NO | – | – | $v_{\rm opt} = 22,800$ |
| 17 | 11 20 52.62 | −0 00 07.7 | 18.7 | 23.7 | 4.0 | Spheroidal, ND | – | – | – |
| 18 | 11 39 57.79 | −0 16 29.7 | 20.2 | 25.7 | 5.0 | Spheroidal, ND | – | – | |
| 19 | 11 41 07.52 | −0 10 00.6 | 18.8 | 24.3 | 5.0 | Spiral | 9.5 | 45 | $v_{\rm H\,I} = 11{,}901$ |
| 20 | 11 43 21.01 | 0 01 43.1 | 18.4 | 23.4 | 4.0 | ?, NO | – | – | $v_{\rm opt} = 5643$ |
| 21 | 11 55 58.49 | 0 02 36.2 | 19.2 | 24.2 | 4.0 | Irr | 9.1 | 90 | $v_{\rm H\,I} = 7791$ |
| 22 | 12 00 47.67 | −0 01 23.2 | 16.3 | 23.0 | 9.0 | NGC4030b, NO | – | – | $v_{\rm opt} = 1878$ |
| 23 | 12 01 43.69 | −0 11 03.6 | 17.1 | 23.3 | 6.0 | ?, NO | – | – | $v_{\rm opt} = 44,937$ |
| 24 | 12 07 10.38 | −0 15 34.1 | 18.1 | 23.6 | 5.0 | Spiral, NO | – | – | $v_{\rm opt} = 6735$ |
| 25 | 12 19 30.21 | −0 13 15.3 | 19.4 | 24.4 | 4.0 | Spheroidal, ND | – | – | – |
| 26 | 12 21 02.48 | 0 00 22.4 | 19.1 | 24.1 | 4.0 | Irr | 8.6 | 83 | $v_{\rm H\,I} = 6224$ |
| 27 | 12 23 42.18 | −0 15 25.8 | 17.4 | 23.7 | 7.0 | Spiral | 9.0 | 117 | $v_{\rm H\,I} = 7509$ |
| 28 | 12 24 30.78 | 0 04 15.9 | 16.7 | 23.4 | 9.0 | Irr | 8.6 | 83 | $v_{\rm H\,I} = 2062$, $v_{\rm opt} = 4642$ |
| 29 | 12 39 47.62 | 0 02 28.8 | 18.1 | 24.9 | 9.0 | Irr, ND | – | – | – |
| 30 | 12 46 53.10 | −0 09 15.2 | 19.6 | 24.6 | 4.0 | Spheroidal, ND | – | – | |
| 31 | 12 50 04.79 | −0 13 56.6 | 17.6 | 24.4 | 9.0 | Spheroidal | 6.3 | 29 | $v_{\rm H\,I} = 754$ |
| 32 | 12 50 45.22 | 0 03 44.8 | 18.1 | 23.1 | 4.0 | ?, NO | – | – | $v_{\rm opt} = 14,400$ |
| 33 | 12 52 34.05 | −0 10 04.0 | 18.4 | 23.4 | 4.0 | Irr | 7.0 | 98 | $v_{\rm H\,I} = 1018$, $v_{\rm opt} = 1077$ |
| 34 | 13 18 49.53 | 0 04 07.6 | 21.0 | 26.0 | 4.0 | ? | 6.9 | 24 | $v_{\rm H\,I} = 2340$ |
| 35 | 13 24 56.17 | −0 08 02.0 | 18.0 | 23.0 | 4.0 | Spiral, NO | – | – | $v_{\rm opt} = 19,949$ |
| 36 | 13 38 42.60 | −0 15 11.7 | 17.5 | 23.4 | 6.0 | ?, NO | – | – | $v_{\rm opt} = 5940$ |
| 37 | 13 45 56.03 | −0 01 32.0 | 20.7 | 25.7 | 4.0 | ?, ND | – | – | – |
| 38 | 13 50 00.79 | 0 03 43.8 | 20.0 | 25.0 | 4.0 | Irr, ND | – | – | – |
| 39 | 13 56 23.88 | −0 07 50.3 | 19.6 | 25.1 | 5.0 | Irr, ND | – | – | – |
| 40 | 13 55 22.78 | −0 00 02.7 | 20.9 | 26.0 | 4.0 | ?, ND | – | – | – |
| 41 | 13 59 47.85 | −0 01 53.9 | 18.5 | 24.0 | 5.0 | Spiral, ND | – | – | – |
| 42 | 14 04 55.97 | −0 08 17.2 | 20.5 | 25.5 | 4.0 | Irr | 8.1 | 148 | $v_{\rm H\,I} = 3728$ |
| 43 | 14 06 36.73 | 0 03 55.5 | 19.2 | 24.2 | 4.0 | ? | 8.8 | 97 | $v_{\rm H\,I} = 7335$ |
| 44 | 14 07 44.70 | 0 04 16.0 | 19.2 | 24.2 | 4.0 | Spheroidal, NO | – | – | $v_{\rm opt} = 93,680$ |
| 45 | 14 11 55.22 | 0 04 35.7 | 18.2 | 23.2 | 4.0 | ?, NO | – | – | $v_{\rm opt} = 11,670$ |
| 46 | 14 14 16.57 | −0 15 34.3 | 18.5 | 23.5 | 4.0 | ?, NO | – | – | $v_{\rm opt} = 11,610$ |
| 47 | 14 20 33.93 | −0 09 17.6 | 18.1 | 23.6 | 5.0 | Spheroidal | 7.4 | 6.3 | $v_{\rm H\,I} = 1610$, $v_{\rm opt} = 1574$ |
| 48 | 14 24 03.96 | 0 03 58.5 | 18.2 | 23.2 | 4.0 | Spiral, NO | – | – | $v_{\rm opt} = 46,655$ |
| 49 | 14 36 53.51 | −0 14 54.3 | 18.4 | 23.4 | 4.0 | ?, NO | – | – | $v_{\rm opt} = 30,231$ |
| 50 | 14 38 43.43 | −0 04 48.4 | 19.2 | 24.9 | 4.0 | Irr, ND | – | – | – |
| 51 | 14 39 59.91 | −0 11 10.2 | 17.6 | 23.4 | 6.0 | Irr | 8.4 | 244 | $v_{\rm H\,I} = 1859$ |

The filters were designed to detect exponential disc objects, and to give an output of zero if convolved with an empty image area (i.e a constant). After the image is cleaned, it is convolved with the filters, giving an output of convolved images on which objects of different sizes are enhanced depending on the filter size. A final image is then built up which has pixel values that are equal to the maximum value assumed in the series of convolved images. So, in this image, all the objects corresponding to the different sizes of filters are emphasized at once.

(iv) For the classification of candidates, possible dwarf and LSB galaxies are identified by selecting all peaks that are $2\sigma$ above the residual noise fluctuations in the final convolved image.

(v) The next step is eye-ball confirmation. Occasionally the detection algorithm picks out possible candidates which are obviously

Downloaded from https://academic.oup.com/mnras/article/352/2/478/1011536 by guest on 23 February 2023

**Table 2.** Table of detections in the UMa cluster.

| Index | RA ($^{h\,m\,s}$) | Dec. ($^{\circ\,\prime\,\prime\prime}$) | $\mu_0$ | Scalelength | Type | Comments |
|---|---|---|---|---|---|---|
| 1 | 12 04 54 | 45 07 37 | 25.30 | 6.0 | Irr | |
| 2 | 12 04 00 | 45 24 32 | 26.19 | 4.0 | Spheroidal | |
| 3 | 12 06 26 | 42 26 07 | 23.15 | 6.0 | Spiral | MAPS galaxy |
| 4 | 12 19 39 | 49 20 28 | 23.78 | 4.0 | Unsure | |
| 5 | 11 39 28 | 47 34 13 | 24.02 | 5.0 | Unsure | PC 1136 + 4750$z = 0.014\,243$ |
| 6 | 11 41 12 | 47 38 18 | 24.53 | 4.0 | Spheroidal | |

not dwarf or LSB galaxies, i.e the halo surrounding a bright star, or the path of a satellite. These detections are removed from the list of possible candidates once confirmed by eye.

(vi) In order to measure the photometric parameters, photometry of the objects can be obtained from the peak value of the output image and the size of the best fitting filter.

(vii) The selection criteria are applied to the final catalogue of objects to preferentially pick out dwarf LSB galaxies (see below).

### 3.1 Millennium Galaxy strip selection criteria

Our main objective is to compare the LSB dwarf galaxy population in different environments. To this end, we need consistency in the types of objects we select. This is difficult if the types of objects in different environments are themselves very different. Current wisdom would describe the cluster population as dominated by rather featureless dwarf elliptical (dE) galaxies and the field by irregular galaxies (dIrrs). Even so, to try and be as consistent as possible we have used the same selection criteria for each environment observed. These criteria (central surface brightness, $23 \leqslant \mu_0 \leqslant 26 B\mu$, exponential scalelength, $3 \leqslant h \leqslant 9$ arcsec) were originally chosen following simulations carried out by Sabatini et al. (2003). The simulations were based on the following method (for further details see their paper); a conical volume of Universe (using $\Omega_{\rm M} = 0.3$, $\Omega_{\Lambda} = 0.7$, $h_{100} = 0.75$) was randomly populated with galaxies according to a given LF and surface brightness–magnitude relation (Driver 1999). In addition to this background Universe, a cluster of galaxies was then simulated at the same distance as the Virgo cluster, but with the faint-end slope of the LF left as a free parameter so it could be varied in different runs. The output of the two simulations was a catalogue of galaxies for both the background and the cluster, providing information about, among other things, the redshift, magnitude, scalelength and surface brightness of the 'background' and cluster galaxies. By applying different selection criteria to both the background and cluster galaxy samples, it was possible to determine the best criteria which would maximize the detection of cluster dwarfs and minimize the contamination by background galaxies. The criteria of $\mu_0 \geqslant 23 B\mu$, $h \geqslant 3$ arcsec was found to be the best for such a simulation. The method used to determine the background sky on the CCD frames also meant that there was an upper limit of 9 arcsec to the size of objects detected using this method. The $1\sigma$ surface brightness limit was approximately $26 B\mu$ (see Sabatini et al. 2003). These criteria lead to a detection parameter space of $23 \leqslant \mu_0 \leqslant 26\, B\mu$ and $-10 \geqslant M_B \geqslant -14$ for the Virgo sample. Some objects marginally fainter than $\mu_0 = 26$ were included in the sample and one was demonstrated to be real via an H I detection.

The above selection criteria and simulations were optimized for a cluster of galaxies at approximately the distance of Virgo. For the MGS, however, the data obtained are not all from an overdensity of galaxies concentrated at one distance. However, we still want to detect, for direct comparison, dwarf galaxies with the same intrinsic properties of magnitude and surface brightness as those in the Virgo cluster. The faintest galaxy ($M_B = -10$) will, according to the surface brightness magnitude relation

$$(\mu_0 \approx 0.6 M_B \pm 0.1 + 32 \pm 1.3) \qquad (1)$$

of Driver (1999), have a scale size of $h \approx 3$ arcsec at a distance of 21 Mpc. Thus, within this distance we expect to be able to detect all galaxies with intrinsic properties the same as those detected in the Virgo cluster survey using the same selection criteria. The Virgo cluster lies at a mean distance of about 16 Mpc but probably extends to 21 Mpc (Jerjen et al. 2004). Thus, if we restrict our analysis for the MGS to within 21 Mpc, we are able to detect exactly the same types of objects (magnitudes and surface brightnesses) as we detected in our Virgo cluster survey. We can therefore make a direct comparison between the two very different environments.

We have run the same 'background' simulation as Sabatini et al. (2003) to try and estimate how many 'background' galaxies would contaminate a sample of galaxies selected in this way. A cone of Universe was randomly populated with galaxies using various faint-end slopes of the LF ($\alpha = -1.0$ to $-2.0$) but keeping $\phi$ (=0.0068 Mpc$^{-3}$) and $M_B^*$ ($= -20.3$) constant (Norberg et al. 2002) and using the above surface brightness–magnitude relation. The selection criteria were then applied to the output catalogue of galaxies ($23 \leqslant \mu_0 \leqslant 26\, B\mu$ and $3 \leqslant h \leqslant 9$ arcsec) and we were then able to see over what distances we detected galaxies and what percentage of those galaxies also satisfied $-10 \geqslant M_B \geqslant -14$. Fig. 2 shows a plot of the distribution of numbers of selected objects ($23 \leqslant \mu_0 \leqslant 26\, B\mu$ and $3 \leqslant h \leqslant 9$ arcsec) with increasing distance and different faint-end LF slopes. As can be seen, the numbers grow with distance until approximately 20 Mpc, so the selection criteria restrict the numbers of distant galaxies included in the sample, as required. In Fig. 3 we show how the percentage of selected objects, which also satisfy the absolute magnitude criteria, changes for different LF faint-end slopes. The model predicts that between 25 and 55 per cent of the galaxies detected will have the same intrinsic properties as those detected in the Virgo cluster sample, and lie within 21 Mpc. We can then use these percentages and the number of bright galaxies within the same volume to estimate the relative number of dwarf to giant galaxies within 21 Mpc and compare this to the Virgo cluster result (see below). The current most comprehensive observations of the field galaxy LF (Blanton et al. 2001; Norberg et al. 2002) give a faint-end slope for the field galaxy LF of $-1.2$. For this LF faint-end slope, approximately 35 per cent of our detections are expected to have the same intrinsic photometric properties as the Virgo cluster sample and lie within 21 Mpc. We can also use the simulation to predict the numbers of galaxies detected per deg$^2$ for each LF faint-end slope $\alpha$ and compare this to the observations (Table 4).



Downloaded from https://academic.oup.com/mnras/article/352/2/478/1011536 by guest on 23 February 2023

**Table 3.** Table of unsure detections in the MGS. ND in the comments column means observed but not detected at 21 cm. Object 48 is a marginal detection that will need confirmation.

| Index | RA (J2000) ($^{h\,m\,s}$) | Dec. (J2000) ($^{\circ\,\prime\,\prime\prime}$) | $\mu_0$ | Scalelength (arcsec) | Comments | log $M_{\rm H\,I}$ ($M_\odot$) | $W_{50}$ (km s$^{-1}$) | Velocity (km s$^{-1}$) |
|---|---|---|---|---|---|---|---|---|
| 1 | 10 08 24.06 | −0 08 13.7 | 25.5 | 7.0 | Clumpy | – | – | – |
| 2 | 10 08 24.33 | −0 00 44.1 | 26.0 | 7.0 | Clumpy | – | – | – |
| 3 | 10 08 43.39 | −0 03 15.0 | 25.7 | 5.0 | Clumpy | – | – | – |
| 4 | 10 08 07.72 | 0 00 14.2 | 26.0 | 5.0 | Clumpy | – | – | – |
| 5 | 10 10 05.13 | 0 01 54.2 | 26.2 | 6.0 | V. faint looks like disc-shape, ND | – | – | – |
| 6 | 10 12 42.23 | −0 15 57.0 | 26.2 | 7.0 | Blank sky? | – | – | – |
| 7 | 10 24 25.28 | −0 10 57.3 | 25.6 | 4.0 | Clumpy | – | – | – |
| 8 | 10 23 36.23 | −0 15 40.1 | 25.8 | 5.0 | Clumpy | – | – | – |
| 9 | 10 29 22.06 | −0 10 12.4 | 26.2 | 5.0 | V. faint | – | – | – |
| 10 | 10 29 23.10 | −0 12 22.0 | 25.9 | 4.0 | V. faint but good profile, ND | – | – | – |
| 11 | 10 38 23.67 | 0 01 47.2 | 26.5 | 6.0 | Clumpy | – | – | – |
| 12 | 10 44 26.21 | 0 02 25.1 | 26.1 | 6.0 | Clumpy | – | – | – |
| 13 | 10 44 43.43 | −0 15 09.9 | 25.9 | 4.0 | FPG? | – | – | – |
| 14 | 10 43 28.92 | 0 00 29.3 | 26.4 | 6.0 | Clumpy with cloud?, ND | – | – | – |
| 15 | 10 50 52.50 | 0 04 56.9 | 25.9 | 4.0 | Clumpy | – | – | – |
| 16 | 11 00 40.76 | −0 00 25.6 | 26.2 | 7.0 | Dot | – | – | – |
| 17 | 11 02 37.44 | −0 15 45.0 | 26.0 | 4.0 | Clumpy | – | – | – |
| 18 | 11 04 31.47 | −0 07 43.4 | 25.9 | 6.0 | Unsure, ND | – | – | – |
| 19 | 11 16 22.88 | −0 02 12.6 | 25.4 | 9.0 | Faint pair of galaxies within 0.2′ | – | – | – |
| 20 | 11 18 17.20 | −0 01 23.1 | 26.0 | 4.0 | V. faint, ND | – | – | – |
| 21 | 11 02 37.41 | −0 15 45.2 | 26.4 | 7.0 | Clumpy | – | – | – |
| 22 | 11 04 31.47 | −0 07 43.0 | 25.9 | 4.0 | Clumpy | – | – | – |
| 23 | 11 18 44.61 | −0 10 43.9 | 25.6 | 7.0 | Faint pair of galaxies within 0.1′ | – | – | – |
| 24 | 11 23 48.90 | −0 16 09.6 | 24.9 | 7.0 | Clumpy | – | – | – |
| 25 | 11 23 21.00 | −0 03 19.7 | 26.3 | 6.0 | Faint but good profile, ND | – | – | – |
| 26 | 11 28 29.10 | −0 08 09.0 | 26.1 | 7.0 | Clumpy | – | – | – |
| 27 | 11 33 39.30 | −0 15 27.6 | 26.3 | 6.0 | Dot | – | – | – |
| 28 | 11 37 16.75 | 0 02 36.6 | 26.1 | 5.0 | Dot, ND | – | – | – |
| 29 | 11 38 47.57 | −0 06 37.3 | 25.7 | 4.0 | Clumpy, ND | – | – | – |
| 30 | 11 58 19.36 | −0 01 39.5 | 25.5 | 4.0 | Clumpy | – | – | – |
| 31 | 12 19 42.74 | 0 05 09.6 | 25.8 | 5.0 | Clumpy, ND | – | – | – |
| 32 | 12 34 13.75 | −0 16 30.8 | 26.5 | 7.0 | Dot, ND | – | – | – |
| 33 | 12 45 32.92 | 0 00 09.0 | 26.37 | 6.0 | Unsure, ND | – | – | – |
| 34 | 12 49 32.11 | −0 02 00.5 | 26.3 | 4.0 | V. faint clumpy | – | – | – |
| 35 | 12 54 35.98 | −0 02 39.6 | 26.2 | 4.0 | Unsure, ND | – | – | – |
| 36 | 12 58 37.48 | −0 10 08.7 | 26.1 | 5.0 | Clumpy, ND | – | – | – |
| 37 | 13 03 22.26 | −0 00 06.0 | 26.0 | 4.0 | Clumpy | – | – | – |
| 38 | 13 05 23.59 | 0 00 00.7 | 26.3 | 5.0 | Sph, ND | – | – | – |
| 39 | 13 09 51.20 | −0 12 44.5 | 25.1 | 6.0 | SDSS galaxy cluster | – | – | $v_{\rm opt} = 90, 941$ |
| 40 | 13 13 45.49 | −0 04 32.4 | 26.2 | 6.0 | Clumpy, ND | – | – | – |
| 41 | 13 30 24.09 | −0 03 25.3 | 26.3 | 7.0 | Clumpy | 8.4 | 164 | $v_{\rm H\,I} = 5127$ |
| 42 | 13 38 05.01 | −0 09 01.3 | 25.7 | 4.0 | V. faint clumpy | – | – | – |
| 43 | 13 45 59.37 | −0 04 47.2 | 26.3 | 5.0 | V. faint clumpy, ND | – | – | – |
| 44 | 13 45 53.75 | −0 02 48.7 | 26.4 | 5.0 | V. faint clumpy | – | – | – |
| 45 | 13 46 07.18 | −0 16 54.8 | 23.1 | 4.0 | SDSS galaxy | – | – | $v_{\rm opt} = 57, 807$ |
| 46 | 13 50 20.97 | 0 01 02.4 | 26.6 | 7.0 | V. faint, ND | – | – | – |
| 47 | 13 50 10.85 | −0 02 28.8 | 26.2 | 4.0 | V. faint clumpy | – | – | – |
| 48 | 14 05 38.08 | −0 08 18.7 | 25.9 | 4.0 | Clumpy | 6.4 | 28 | $v_{\rm H\,I} = 940$ |
| 49 | 14 06 14.44 | 0 02 39.8 | 25.8 | 4.0 | V. faint dot | – | – | – |
| 50 | 14 05 41.01 | 0 02 13.0 | 26.1 | 5.0 | Clumpy | – | – | – |
| 51 | 14 15 16.70 | −0 03 22.4 | 25.7 | 4.0 | Clumpy, ND | – | – | – |
| 52 | 14 18 48.79 | −0 02 46.4 | 25.9 | 9.0 | Clumpy | – | – | – |
| 53 | 14 20 57.95 | 0 04 46.0 | 26.0 | 4.0 | Clumpy, ND | – | – | – |
| 54 | 14 20 42.42 | −0 04 02.2 | 26.1 | 7.0 | Clumpy, ND | – | – | – |
| 55 | 14 26 17.75 | 0 03 42.9 | 25.4 | 4.0 | Clumpy | – | – | – |
| 56 | 14 35 47.58 | 0 03 00.8 | 25.8 | 5.0 | clumpy with cloud?, ND | – | – | – |
| 57 | 14 37 23.96 | 0 01 05.4 | 26.0 | 5.0 | Dot v. good profile, ND | – | – | – |
| 58 | 14 40 21.50 | −0 03 51.2 | 25.7 | 5.0 | Clumpy, ND | – | – | – |
| 59 | 14 46 10.43 | 0 02 47.4 | 24.6 | 4.0 | SDSS galaxy | – | – | $v_{\rm opt} = 86, 229$ |

Downloaded from https://academic.oup.com/mnras/article/352/2/478/1011536 by guest on 23 February 2023

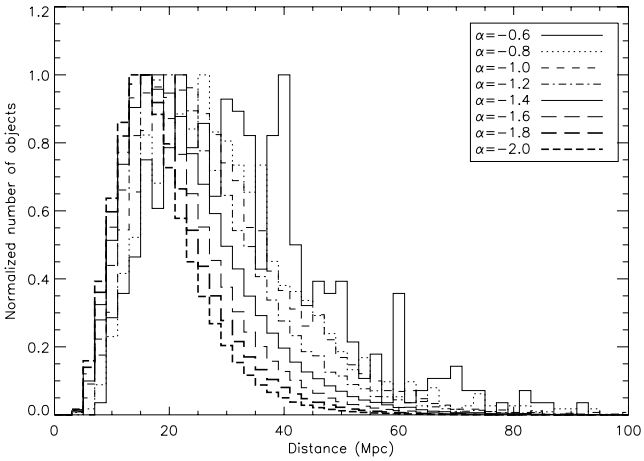


**Figure 2.** Distribution of distances for selected objects with properties in the range $23 \leqslant \mu_0 \leqslant 26 B\mu$ and $3 \leqslant h \leqslant 9$ arcsec at increasing distance for varying values of $\alpha$.

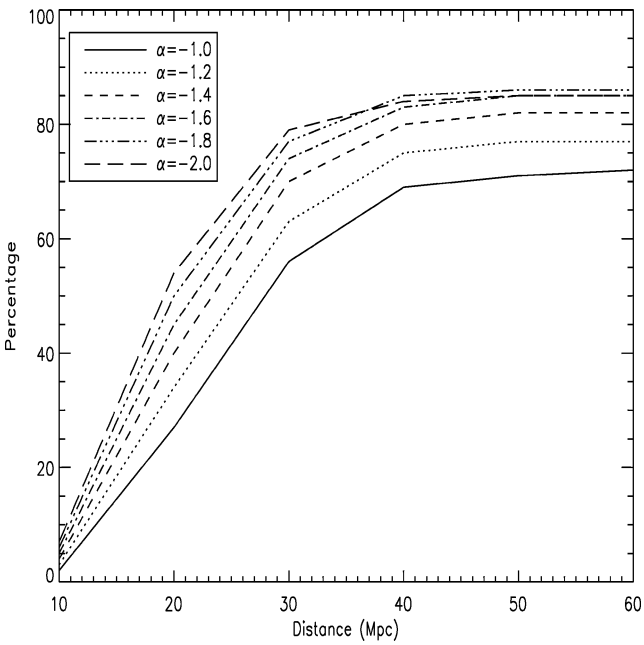


**Figure 3.** Percentage of selected galaxies having intrinsic properties in the range $23 \leqslant \mu_0 \leqslant 26\ B\mu$ and $-10 \geqslant M_B \geqslant -14$ at increasing distance for varying values of $\alpha$.

### *3.1.1 Influence of seeing*

Although our chosen numerical simulation selection criteria for finding LSB dwarf galaxies was $23 \leqslant \mu_0 \leqslant 26\ B\mu$ and $3 \leqslant h \leqslant 9$ arcsec, this was a rather idealized situation. In reality, the frames are influenced by the seeing and in some cases this was quite bad. Fig. 4 illustrates how the seeing influenced the number of detections made in the UMa data. The number of detections increases rapidly as the seeing degrades above about 2.5 arcsec and stars are smeared out into diffuse objects. For this reason, we restricted our three data sets to frames that had a measured seeing of less than 2.5 arcsec (the median seeing of the MGS data was 1.3 arcsec and for the Virgo data set was ≈1.9 arcsec). We have also considered the influence the seeing has on the measured scale size of galaxies. We experimented convolving simulated galaxies with a 3-arcsec scale size with a 1.5–2.5 arcsec Gaussian seeing function. The result was a measured scale size of the order of 4 arcsec. Thus, galaxies with intrinsic scale sizes of 3 arcsec will have measured scale sizes of approximately 4 arcsec. So our final image selection criteria was $23 \leqslant \mu_0 \leqslant 26 B\mu$, $4 \leqslant h \leqslant 9$ arcsec. Sabatini et al. (2003) demonstrate that these selection criteria successfully select Virgo cluster dwarf galaxies.

**Table 4.** The predicted number of objects detected with $23 \leqslant \mu_0 \leqslant 26\ B\mu$ and $3 \leqslant h \leqslant 9$ arcsec for each LF faint-end slope $\alpha$.

| $\alpha$ | No objects per deg$^2$ |
|---|---|
| −0.6 | 0.005 |
| −0.8 | 0.02 |
| −1.0 | 0.1 |
| −1.2 | 0.2 |
| −1.4 | 1 |
| −1.6 | 5 |
| −1.8 | 24 |
| −2.0 | 127 |

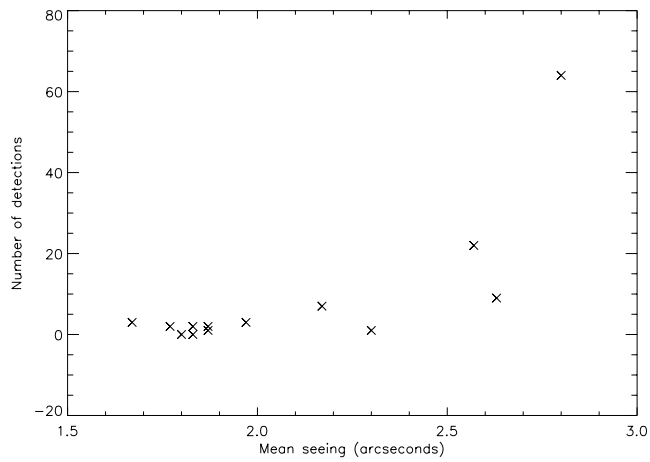


**Figure 4.** How seeing affected the number of detections.

## 3.2 *B–i* colours

In our previous work (Sabatini et al. 2004) we looked at the (*B–i*) colours of LSB dwarf galaxies in environments of increasing density. It was evident that as the density increased, the galaxies became redder, indicating a strong environmental effect on the stellar population of these galaxies. However, the data for this comparison were taken from surveys selected in different ways. To check the results of the comparison, therefore, we have obtained colours for the four objects within 21 Mpc from Data Release 1 of the SDSS. In Sabatini et al. (2004), the colours given were (*B–i*), thus we converted the *g* colour of our objects to *B* using the conversion equation given by Cross et al. (2004)

$$B = g + 0.39(g - r) + 0.21, \tag{2}$$

and we calculated (*B–i*) using the calculated *B* values and the *i* magnitudes from the SDSS. The results are shown in Section 4.3



Downloaded from https://academic.oup.com/mnras/article/352/2/478/1011536 by guest on 23 February 2023

## 4 RESULTS

### 4.1 Millennium Galaxy strip – optical detections

We applied the detection and measurement algorithm described above to 30 deg$^2$ of data from the MGS. The algorithm found 110 objects, each of which was confirmed by eye. In the main, the detected objects are very different to those detected in our Virgo cluster survey. The Virgo cluster survey detections are predominately smooth diffuse objects (dE galaxies). In the field, a large fraction of the detections are rather 'clumpy' objects and it is much more difficult to distinguish between what might be groups of faint distant objects from nearby irregular galaxies. For this reason, we have divided our list of detections into two groups: those we are sure are individual galaxies and those that we are less confident of (Tables 1 and 3). Examples from Tables 1 and 3 are shown in Figs 5 and 6. For our sure detections, we have 51 objects corresponding to 1.7 per deg$^2$. Including the less sure objects gives 3.6 per deg$^2$. Comparing this with Table 4 shows that this is consistent with a LF faint-end slope of the order of $\alpha = -1.4$. Note that the Virgo cluster survey detected an average of 20 dwarf galaxies per deg$^2$ varying from about 40 per deg$^2$ at the cluster centre to 4 per deg$^2$ at the cluster edge.

Given that the numbers per deg$^2$ indicate that $\alpha \approx -1.4$ the model predicts (Fig. 3) that ≈45 per cent of our detections should have intrinsic photometric properties the same as those detected in the Virgo cluster and lie within 21 Mpc. We should have about 23 (50) objects satisfying this requirement in our sample. Henceforth, numbers in brackets are if we include the less sure objects from Table 3.

As we were dealing with small numbers, in Sabatini et al. (2003) we defined and used a dwarf-to-giant number ratio (DGR) rather than a LF faint-end slope. We defined the DGR as the number of dwarfs with $-10 \geqslant M_B \geqslant -14$ and $23 \leqslant \mu_0 \leqslant 26 B\mu$ divided by the number of galaxies with $M_B \leqslant -19$.

We can use the DGR and the initial results for the MGS to compare with other data; if we integrate the 2dF LF of Norberg et al. (2002) between $-10 \geqslant M_B \geqslant -14$ and $-19 \geqslant M_B \geqslant -24$ we find a DGR of 18. For a steeper LF consistent with CDM simulations

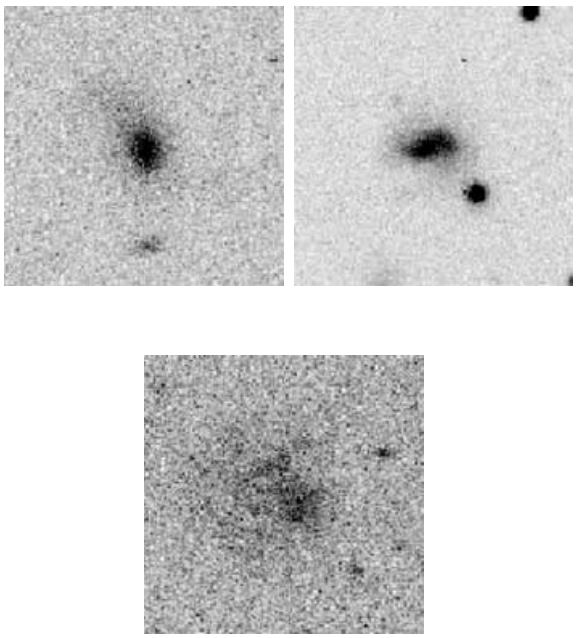

**Figure 5.** Examples of objects easily classified as galaxies (from Table 1).

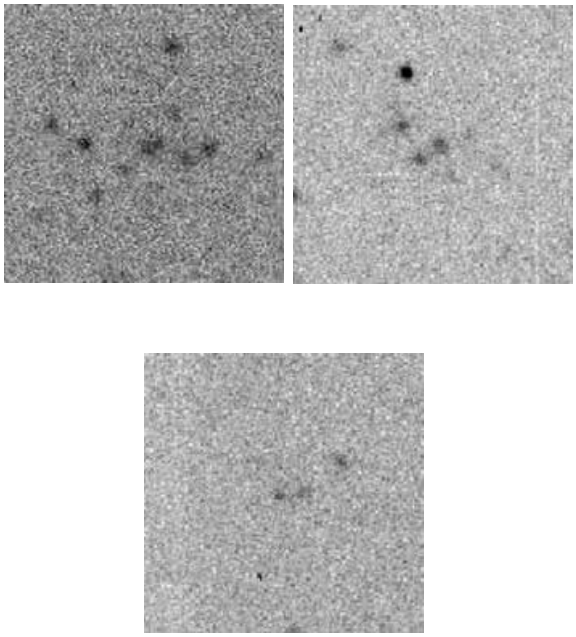

**Figure 6.** Example of objects classified as 'unsure detections' (from Table 3). One object very similar to the above has been confirmed via an H I detection as a Virgo cluster dIrr galaxy.

**Table 5.** Table of results for the surveys and simulations.

| Survey/simulation | DGR |
|---|---|
| Virgo cluster | 20 : 1 |
| Local Group | 5 : 1 |
| LF ($\alpha = -0.6$) | 0.24 : 1 |
| LF ($\alpha = -0.8$) | 1 : 1 |
| LF ($\alpha = -1.0$) | 4 : 1 |
| LF ($\alpha = -1.2$) | 18 : 1 |
| LF ($\alpha = -1.4$) | 80 : 1 |
| LF ($\alpha = -1.6$) | 367 : 1 |
| LF ($\alpha = -1.8$) | 1735 : 1 |
| LF ($\alpha = -2.0$) | 8371 : 1 |

($\alpha = -1.6$ to $-2.0$, but keeping $M_B^*$ constant) we have DGRs in the range 367 : 1 to 8371 : 1. Note that this is for galaxies of all surface brightnesses. For the LG we have DGR ≈5. If we subtract the predicted four per deg$^2$ background contaminating galaxies from the Virgo data, we have DGR = 20. This is all summarized in Table 5. The model described in Section 3.1 predicts that there should be only 0.3 galaxies in our sample with $M_B \leqslant -19$ and $d < 21$ Mpc. For $\alpha = -1.5$ it predicts 51 dwarf galaxies within 21 Mpc with $23 \leqslant \mu_0 \leqslant 26\ B\mu$ and $-10 \geqslant M_B \geqslant -14$. The latter number is consistent with our observations (45 per cent of 110 detections is 50), but see below.

We have used the NED to find all those catalogued galaxies within our survey area that lie within 21 Mpc and have $M_B \leqslant -19$. There are six galaxies that satisfy the above criteria. As stated above, our simulation predicts that there should be 0.3. Thus, the volume sampled by the MGS to 21 Mpc is overdense in bright galaxies, compared to our simulation, by about a factor of 20. This illustrates the difficulty of finding a 'typical' region of the Universe. Although the region sampled by the MGS is less dense than the Virgo cluster, it is more dense than that sampled by the large area redshift surveys



Downloaded from https://academic.oup.com/mnras/article/352/2/478/1011536 by guest on 23 February 2023

that provided the data for our simulation. The main reason for this overdensity is that the MGS crosses the Virgo Southern Extension. Four of the six bright galaxies reside in this region. Thus, if all of our 110 detections were to lie within 21 Mpc we would have a DGR of 18 ($\alpha \approx -1.2$). As we will show below, only a small fraction of our detected galaxies actually reside within 21 Mpc and so the LF of this particular region of the Universe has a very flat faint-end slope even when observed to the very LSB levels of our survey.

### 4.2 Redshifts and H I detections

We have 19 (22) optical redshifts (Driver, private communication) for our galaxy detections. None of these lies within 21 Mpc, which corresponds to $v_{\rm opt} = 1575$ km s$^{-1}$ assuming that velocities can be directly converted into distance. This should be a reasonably accurate assumption, as the peculiar velocity of one of the giant galaxies within 21 Mpc, which had a Tully–Fisher distance, was only $\approx$10 km s$^{-1}$. During our two Arecibo observing runs, we obtained a further 16 (18) H I detections, 4 (5) of which lie within 21 Mpc (Nos 12, 13, 31 and 33 from Table 1 and No 48 of Table 3). Objects 12 and 13 are separate optical sources, but they lie in the same Arecibo beam. We are assuming, by their close association on the sky and their appearance, that they are both at the distance indicated by the 21-cm velocity. Object 12 also has an optical redshift coincident with the H I detection. We would not have believed the H I detection without this correspondence. We will assume that the H I detected in the Arecibo beam is associated predominately with the brighter object (12). It has the appearance of a dSph galaxy and a very small H I mass that is only detected because of its narrow velocity width (Table 1). With $M_B = -13.3$ it has a very low mass-to-light ratio of $M_{\rm H\,I}/L_B = 0.05$. Object 13 is fainter at $M_B = -10.0$ and, as far as is possible to see, it also has the smooth appearance of a dSph galaxy. Object 31 again appears to be a spheroidal with a low H I mass. It has $M_B = -12.4$ and $M_{\rm H\,I}/L_B = 0.15$ and again the small amount of atomic hydrogen is detected because of the small velocity width. Object 33 is of a much more irregular appearance and, as might be expected, has much more atomic hydrogen than the other two, $M_B = -12.4$ and $M_{\rm H\,I}/L_B = 0.8$. There is also one object (No 48), at $v_{\rm H\,I} = 940$ km s$^{-1}$, from Table 3 that is a marginal H I detection. Images of the four objects of Table 1 are shown in Fig. 7; their H I spectra are shown in Fig. 8.

### 4.3 ($B - i$) colours

The ($B$–$i$) colours for the four objects in the MGS within 21 Mpc are given in Table 6. The mean value is 0.95, which is much bluer than the mean value of 1.5 found for the Virgo cluster (Sabatini et al. 2004).

To compare the colours of the above four objects with those objects found in the Virgo cluster by Sabatini et al. (2004), we have plotted the colours against their absolute magnitudes according to their morphologies in Figs 9 and 10. Fig. 9 shows the distribution of the dEs in Virgo and the field, whereas the irregular galaxies are plotted in Fig. 10. Two of the field dEs (objects 12 and 13) are much bluer than those in the Virgo cluster – they lie outside the colour distribution for these objects. The third dE in the field (object 31) lies within the thick band running across the plot. The dIrr (object 33) in the field seems to have a $B$–$i$ colour which is consistent with those of the Virgo cluster dIrrs although the scatter is large. There are a number of Virgo dEs and dIrrs which have a ($B$–$i$) $> 2$, which might indicate that these are high-redshift objects. Because we have no redshift information for these objects, we cannot rule this out.

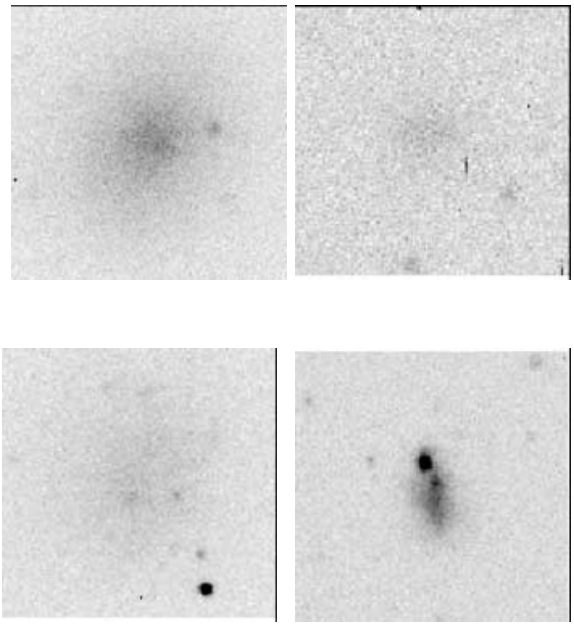

**Figure 7.** The four objects from the MGS detected within 21 Mpc: from top-left to bottom-right, numbers 12, 13, 31 and 33.

However, a check on the colours of the sure detections in Table 1 showed that four of these objects had similar ($B$–$i$) colours of greater than 2, and the only one of these objects which had a redshift (object 42 from Table 1) was not at a particularly large distance.

### 4.4 Association with bright galaxies

The lower plot in Fig. 11 shows a plot in RA of the total number of optical detections along the MGS. The dotted histogram in Fig. 11 includes all the detections we found along the strip (i.e those listed in Tables 1 and 3); the solid histogram includes just those which we list in Table 1. Shown in both plots of Fig. 11 is the approximate position of the Virgo Southern Extension, plotted as a dashed line at approximately 16 Mpc. Interestingly, it appears to be situated just where there is a dip in the total number of detections. It was pointed out by the referee that the total number of detections is higher at both ends of the survey, where the galactic latitude is low, suggesting that some of the unsure detections may be groups of faint stars within the galaxy. The upper plot of Fig. 11 shows the positions along the MGS of the six bright galaxies ($M_B < -19$) within 21 Mpc. We can also see if any of the detected galaxies are possible companions of the brighter galaxies. In the review of Mateo (1998) of the LG, the furthest dwarf galaxy companion of the MW is at a distance of 250 kpc. For each bright galaxy we have indicated this distance on the upper plot of Fig. 11. Numbers 12 and 13 are almost certainly companions of NGC 3521. Number 31 lies in the Virgo Southern Extension but does not seem to be associated with any of the bright galaxies. Number 33 is at about the same velocity as NGC 4517 although the projected separation is a large 1.2 Mpc.

This is a far lower number of companions than might have been expected compared to the MW. If the MW was within 21 Mpc we would expect five companions to be detected. A check was made that the area surrounding the bright galaxies was not masked during the detection phase leading to the removal of nearby companions. We created simulated images of the MW and its companions and added these to real data frames. The detection algorithm picked out all



Downloaded from https://academic.oup.com/mnras/article/352/2/478/1011536 by guest on 23 February 2023

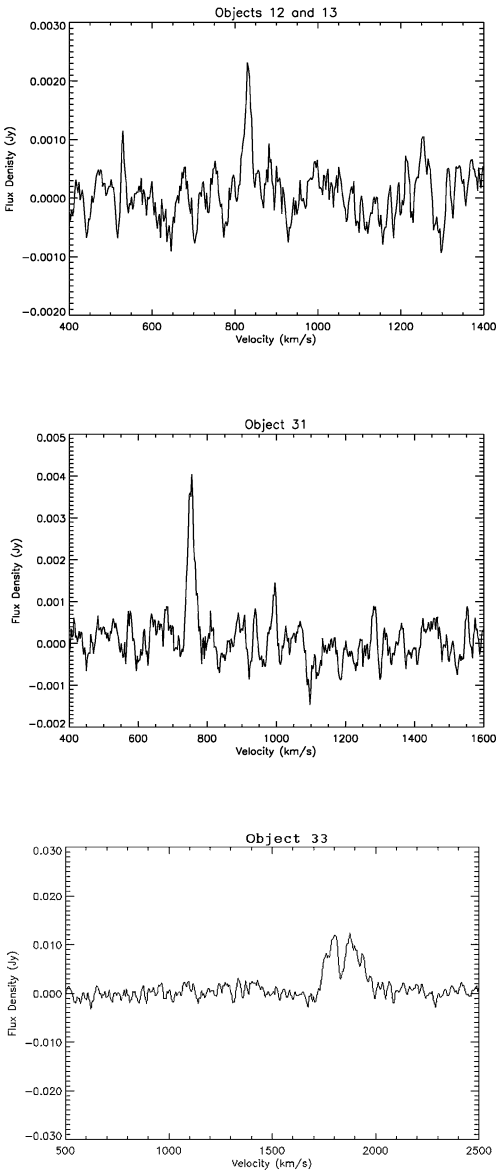


**Figure 8.** H I spectra for the MGS detections within 21 Mpc.

**Table 6.** Table of colours for the MGS objects within 21 Mpc.

| Object number | *B–i* |
|---|---|
| 12 | 0.63 |
| 13 | 0.80 |
| 31 | 1.40 |
| 33 | 0.97 |

of the companions at all distances within 21 Mpc (Sabatini 2003). Thus, either the bright galaxies in our survey region do not have dwarf companions like the MW or they are being hidden in some way, possibly because they are much closer to the galactic disc. The same applies to the Virgo cluster dwarfs – they do not appear to be associated with the bright cluster galaxies (Sabatini et al. 2003). Why we are not finding a similar number of companions to these galaxies as that found around the MW is not at all clear and we are undertaking a more detailed study of the companions of nearby bright spiral galaxies.

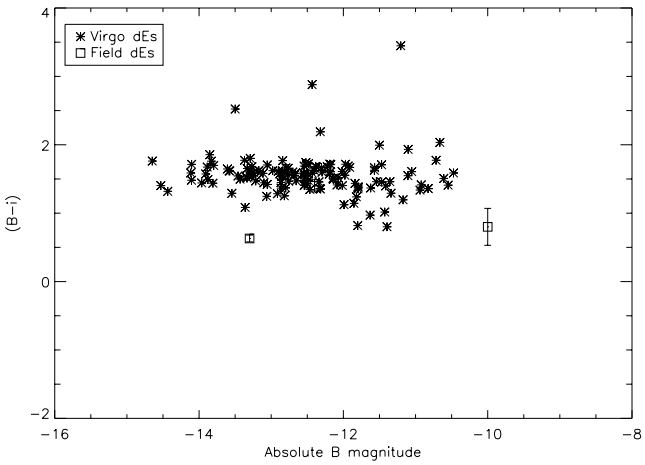


**Figure 9.** *B–i* colours plotted as a function of absolute magnitude for both Virgo cluster and field dE galaxies. Also plotted are the errors in (*B–i*) for the field dEs.

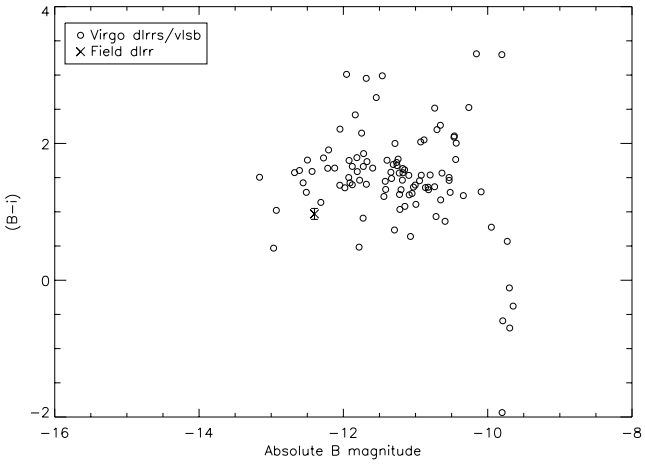


**Figure 10.** *B–i* colours plotted as a function of absolute magnitude for Virgo cluster dIrrs/very LSB and field dIrr. Also plotted are the errors in (*B–i*) for the field dIrr.

### 4.5 Ursa Major

For our small area survey of the UMa cluster, the same detection algorithm was used and the same selection criteria as the MGS and Virgo surveys were applied. Table 2 lists the detections made. The detection with known redshift obtained from the NED shows that this object, situated at approximately 57 Mpc, is outside the cluster. The detections correspond to about four objects per deg$^2$ for UMa, which is in reasonable agreement with the value obtained for the MGS data as a whole. The UMa data are perfectly consistent with observations of the general field showing no enhancement, unlike the Virgo cluster, of dwarf galaxy numbers. Two of the galaxies appear to be morphologically similar to the dominant dE population of the Virgo cluster. There were no bright galaxies in any of the UMa fields so we are not able to calculate a DGR for UMa. So, although UMa is an enhancement of giant galaxies it does not seem to have an enhanced dwarf galaxy population.

Downloaded from https://academic.oup.com/mnras/article/352/2/478/1011536 by guest on 23 February 2023

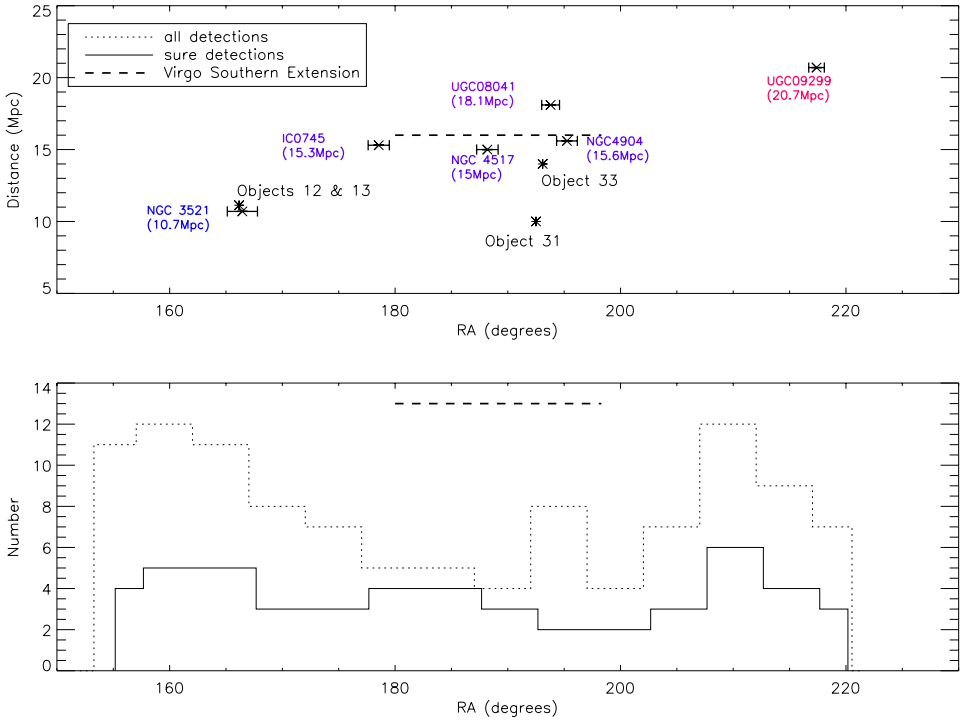


**Figure 11.** The upper figure illustrates the possible association of dwarf galaxies with giant galaxies. The giant galaxies (within 21 Mpc) are labelled on the plot, with the lower galaxies being those which are closer to us, as indicated by the distance scale on the *y*-axis. The size of the error bar on the giant galaxies indicates a projected distance of 500 kpc. The positions of dwarf galaxies with redshifts are also marked. In the lower plot, the dashed histogram is the distribution of all the detections (Tables 1 and 3). The solid histogram shows the distribution of the definite optical detections from Table 1. The approximate extent of the Virgo Southern Extension is shown on both plots as a bold dashed line.

### 4.6 Results summary

34 (39) out of 51 (110) of the objects detected as part of our optical survey of the MGS now have redshifts (distances). It appears that our optical classification as 'sure galaxy' was reasonably good because 66 per cent of the objects in Table 1 have redshifts. For those objects in Table 1, 33 objects were observed at 21 cm (see the caption of Table 1 for comment on those objects in the same telescope beam) and there were 16 detections (48 per cent). For the objects of Table 3 there were 25 objects observed and only two detections (8 per cent) and one of these (No 48) is only a marginal detection.

As stated in Section 3.1, within 21 Mpc we should be able to detect the same range of magnitudes and surface brightnesses as that of our Virgo cluster survey (Sabatini et al. 2004). The Virgo cluster is a well-known large overdensity of bright galaxies, and also has a large overdensity of dwarfs. The MGS data produced just 1.7 (3.7) objects per deg$^2$ while the Virgo fields produced, on average, 20. The sparse UMa data produced numbers per deg$^2$ consistent with the MGS data and not at all similar to the Virgo cluster. The MGS produced just four (five) objects out to 21 Mpc. Scaling by the relative projected areas of the surveys and assuming that the cluster extends to 21 Mpc, Virgo would have produced almost 100. The DGR of Virgo is about 20. At face value (see below) the DGR for the MGS out to 21 Mpc is less than one.

During the Virgo survey we observed 103 galaxies at 21 cm and had just five detections, three of which had velocities consistent with being cluster members. This is a 5 per cent success rate.[2] We observed 33 (58) galaxies at 21 cm from the MGS data and 16 (18) were detected, giving an efficiency of 48 per cent (31 per cent). All four of the objects detected within 21 Mpc were also detected in H I. These observations are obviously consistent with a very different LF for the field (flat) compared to the cluster (steeper). The field galaxy population is also gas-rich compared to that in the cluster. A concern is that in the LG we find a DGR of 5. Have we missed five times as many dwarfs as we have found?

## 5 DISCUSSION

As stated above, only four (five) of the objects with redshifts lie within 21 Mpc. Roughly accounting for those objects without redshifts we can have no more than six (18) objects within 21 Mpc in total. In Section 3.1 we described a model of the numbers expected for various LF faint-end slopes. Given the observed numbers per deg$^2$ we would have expected a LF faint-end slope of about $-1.4$, and so approximately 45 per cent of our detections were predicted to lie within 21 Mpc. This corresponds to 23 (50) objects. This discrepancy leaves us with a bit of a dilemma. As stated in Section 4.1, the volume sampled by the MGS to 21 Mpc is overdense in bright

[2] Given the very much higher surface density of objects detected in the Virgo survey, this must mean that the majority of the objects observed in the Virgo cluster are gas-poor (most likely dE types) and not distant contaminating galaxies (Sabatini et al. 2004) because there were few distant ($v_{\rm H\,I}$> 2000 km s$^{-1}$) detections. The MGS data cover a much larger area than the Virgo data, so we would only expect 20 (44) objects like those in Table 1 to be contaminating the whole Virgo data (which contain a total of 257 galaxies). The majority of galaxies in our Virgo cluster catalogue must be associated with the Virgo cluster.



Downloaded from https://academic.oup.com/mnras/article/352/2/478/1011536 by guest on 23 February 2023

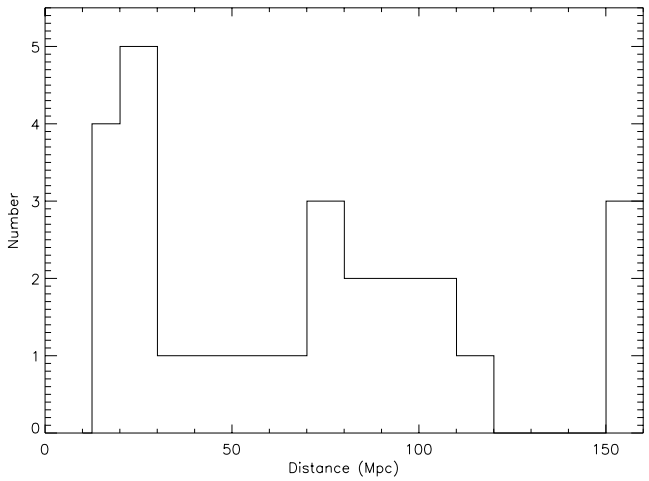


**Figure 12.** The distribution of measured distances.

($M_B < -19$) galaxies by a factor of 20, yet it is certainly underdense in dwarfs ($-14 < M_B < -10$) compared to the model expectations.

The explanation appears to be twofold. First, there are a number of very high redshift objects that the model does not predict should be there. The model does not take account of galaxy evolution. The second reason is that galaxies are not distributed uniformly in the Universe. In Fig. 12 we show the distribution of observed galaxy distances, which can be directly compared with the model predictions of Fig. 2. Although the predicted peak at about 21 Mpc can clearly be seen, there is also an excess of galaxies at distances greater than 70 Mpc. The model has been useful in that it enabled us to clearly specify the problem and to define the consequences of our selection criteria, but now we have the distances to so many objects it is not required for the interpretation of the data.

In the previous section we compared our result to that of the Virgo and UMa clusters. In this section we want to compare with the predictions of CDM galaxy formation models. To do this, we want to be as optimistic as possible about the numbers of objects we might be missing. There are six bright galaxies ($M_B < -19$) within 21 Mpc. We have four dwarf galaxy ($-14 < M_B < -10$) detections (12, 13, 31, 33) within 21 Mpc giving a DGR of 0.7. Including the possible detection of object 48 of Table 3 increases this to 0.8. Adjusting now for the possibility that some of the unobserved and undetected objects lie within 21 Mpc produces a further two possible objects in Table 1 and 11 in Table 3, giving a DGR of 3. Now, in Section 3.1 we said that we can detect all galaxies with $-14 < M_B < -10$ within 21 Mpc. This is actually only true if they follow the Driver (1999) surface brightness relation. At fainter magnitudes some galaxies of higher surface brightness will be missed because they are too small. The volumes over which dwarf galaxies can be detected compared to the volume out to 21 Mpc are listed in Table 7; this is the visibility function.[3]

As can be seen for higher surface brightnesses and fainter magnitudes, we do not sample the whole volume – the objects are too small at larger distances. Our observations do not rule out a population of faint galaxies of higher surface brightness in the field or in the Virgo cluster. Is there any evidence of such a population? Our first comment is that, given the sparse numbers of detections for those magnitudes and surface brightnesses for which we have full volume coverage, the LF would have to do something very strange if the numbers predicted by CDM are to be accounted for. In the LG there are 10 galaxies that satisfy our magnitude and surface brightness selection criteria. Of these, half lie in the region where we do not have full volume coverage. If this was also true for the MGS region, then the DGR would at most double from 3 to 6. Observations by Deady et al. (2002) have been specifically made to try and identify higher surface brightness dwarfs in both the Fornax (Deady et al. 2002) and Virgo clusters (Drinkwater, private communications). In Virgo, this amounts to about 3 per deg$^2$ or about an additional 15 per cent of our original total number. We conclude that there is no large population of higher surface brightness dwarf galaxies that have been missed in the MGS data and that, at most, the DGR is 6.

[3] Note that this does not affect our comparison with the Virgo data because both are observed over a similar depth.

**Table 7.** Relative volumes, expressed as a percentage, that galaxies of different surface brightnesses ($\mu_0$) and magnitudes ($M_B$) can be detected within – the visibility function.

| | $M_B$ | | | | |
|---|---|---|---|---|---|
| $\mu_0$ | −10 | −11 | −12 | −13 | −14 |
| 26 | 99 | 100 | 100 | 100 | 100 |
| 25 | 25 | 99 | 100 | 100 | 100 |
| 24 | 6 | 25 | 99 | 100 | 100 |
| 23 | 2 | 6 | 25 | 99 | 100 |

There is not a large population of faint-field LSB dwarf galaxies that have been missed by the redshift surveys (see also Cross et al. 2001). We have measured the local LF down to 3 mag fainter than the major redshift surveys, which produce LFs that are accurate over the range $M_B < -17$ (Driver & de Propis 2003). With a DGR of, at most 6, the LF is flatter or declining ($\alpha > -1$) compared to an extrapolation of the redshift survey measured faint-end slopes. Within the CDM paradigm, the suppression of star formation in field dwarf galaxies has been extremely efficient.

The observed environmental effect on both the number of dwarf galaxies and their relative number compared to bright galaxies in the field and cluster is completely opposite to that predicted by CDM for dark matter haloes. Lemson & Kauffmann (1999) specifically consider the environmental influences on dark matter haloes and their associated galaxies. They conclude that the halo mass function (LF?) 'is skewed towards high-mass objects in overdense regions of the Universe and towards low-mass objects in underdense regions'. Thus, the CDM simulations predict that the ratio of low to high mass objects in the field should be higher than in clusters, completely opposite to what is observed. However, we must be careful with this comparison. CDM predicts how many dark haloes there should be – this should not be confused with the number of faint galaxies searched for in our surveys. Nevertheless, if these haloes do contain stars, thus making them visible as dwarf galaxies, then a mechanism must be used to suppress their formation in the field in order to reconcile their predicted numbers with observations – this is often referred to in the simulations as a 'feedback' mechanism. The normal 'feedback' mechanism invoked in most models is to expel gas from small dark matter potentials by the injection of energy by the first supernovae. This suppresses the formation of stars in these haloes and they remain undetected (dark). This should apply equally in all environments (Virgo, UMa and the MGS) suppressing the formation of dwarf galaxies everywhere. A possible solution is that the intracluster gas in environments such as Virgo prevents the gas escaping (Babul & Rees 1992). This would only apply to galaxies within the cluster core where the gas density is relatively high,

Downloaded from https://academic.oup.com/mnras/article/352/2/478/1011536 by guest on 23 February 2023

but, within the core, dwarf galaxies are subject to tidal destruction (resulting in intracluster stars, planetary nebulae and intergalactic light; Sabatini et al. 2004). Ram pressure stripping is again only effective in the cluster core and suppresses rather than enhances star formation. Tully et al. (2002) have proposed that the environmental dependence is due to the time at which larger-scale structures form in relation to the epoch of reionization. They propose that the dwarf galaxy population of Virgo formed early, before reionization, and was able to retain gas and form stars. In the lower-density environments (UMa, MGS) the dark matter haloes form later, after reionization, and the gas is too hot to collapse. Tully et al. say that there is only 'qualitative' agreement between their idea and observations. Their argument is further weakened by the recent result by the *Wilkinson Microwave Anisotropy Probe* (*WMAP*) team that places the epoch of reionization at a much more distant redshift of $z \approx 20$ (Kogut et al. 2003).

A test for the existence of dark haloes (dark matter haloes with no stellar systems) would be to use gravitational lensing as a probe of substructure. This is an ideal tool to use because light is deflected gravitationally by matter, whether it is light or dark, thus if there were small dark haloes present in the Universe, they could be detected by this means. Such studies have been carried out (Bradac et al. 2002; Metcalf & Zhao 2002) and preliminary results show evidence for the presence of substructure. Dalal & Kochanek (2002) studied seven four-image lens systems, six of which had flux anomalies which they commented could be due to the effects of substructure. They also rule out the possibilities of other effects causing the flux anomalies in a further study of their data (Kochanek & Dalal 2003), concluding that 'low-mass haloes remain the best explanation of the phenomenon'. However, if these low-mass dark matter haloes do exist in the numbers predicted by CDM, then as they fall through the disc of their parent galaxy, they should heat the disc and cause it to thicken (Tóth & Ostriker 1992; Moore et al. 1999b). This is contrary to some observations of old thin disc systems or galaxies with no thick disc components, although it is now being argued that the amount of heating and thickening has been overestimated (Velázquez & White 1999; Font et al. 2001). This is clearly a matter for further investigation.

The Virgo cluster cannot have been assembled out of objects like the LG without some additional physical mechanism being involved that increases the ratio of dwarf to giant galaxies. Virgo is a very dense environment where many galaxy–galaxy interactions are likely to have occurred due to its short dynamical crossing time compared with UMa ($\approx 0.1 H_0$ and $\approx H_0$, respectively; Trentham et al. 2001; Trentham & Hodgkin 2002). Virgo is also an X-ray cluster, so galaxies in the cluster core move through a relatively dense intergalactic gas. UMa is also probably in a much earlier stage of formation than Virgo. The question is, are these the differences that lead to Virgo being so different?

The large dwarf galaxy population found in Virgo seems to lend some credence to the theory of dwarf galaxy formation by galaxy harassment, an idea put forward by Moore et al. (1999b). In this scenario, dE galaxies are formed when infalling LSB spiral galaxies are harassed in the cluster by the giant galaxies, and lose their gas resulting in a morphological transformation into a dE. Further evidence to support this theory comes from a study of the Virgo cluster dwarfs, conducted by Conselice, Gallagher & Wyse (2001). They show that the dEs found in Virgo have a velocity distribution closer to that of the spirals than that of the earlier-type galaxies. The dwarf velocity distribution is quite wide, and is non-Gaussian with a total velocity dispersion of 726 km s$^{-1}$. This is similar to that of the spirals, which is 776 km s$^{-1}$. The dwarf galaxies appear not to be relaxed and are less dynamically evolved than the Virgo cluster core elliptical population. However, in Sabatini et al. (2004) we show that the dwarf galaxies we detect in the Virgo cluster are too small to be the result of the harassment process proposed by Moore et al. (1999a). We propose that the dE galaxies are the result of an earlier infalling dIrr galaxy population. These galaxies may be associated with the faint blue galaxies seen at higher redshift ($0.5 < z < 1.5$). Sabatini et al. (2004) suggest that the star formation of these small infalling haloes is enhanced by the weak tidal interactions with the cluster potential and other cluster galaxies – these types of interactions are not available to galaxies in UMa or the MGS. These haloes have their evolution advanced by the cluster environment. Maybe small dark matter haloes require these sorts of tidal interactions to light up and reveal their baryons.

## ACKNOWLEDGMENTS

The Arecibo Observatory is part of the National Astronomy and Ionosphere Centre, which is operated by Cornell University under a cooperative agreement with the National Science Foundation. This research also has made use of the Lyon-Meudon Extragalactic Data base (LEDA), recently incorporated in HyperLeda, and the NED, which is operated by the Jet Propulsion Laboratory, California Institute of Technology, under contract with the National Aeronautics and Space Administration (NASA).

Funding for the creation and distribution of the SDSS Archive has been provided by the Alfred P Sloan Foundation, the Participating Institutions, NASA, the National Science Foundation, the US Department of Energy, the Japanese Monbukagakusho, and the Max Planck Society. The SDSS website is http://www.sdss.org/. The SDSS is managed by the Astrophysical Research Consortium (ARC) for the Participating Institutions. The Participating Institutions are the University of Chicago, Fermilab, the Institute for Advanced Study, the Japan Participation Group, Johns Hopkins University, Los Alamos National Laboratory, the Max-Planck-Institute for Astronomy (MPIA), the Max-Planck-Institute for Astrophysics (MPA), New Mexico State University, the University of Pittsburgh, Princeton University, the United States Naval Observatory, and the University of Washington.

Finally, we would like to thank Jochen Liske and Simon Driver for supplying the redshift data for many of our objects, and also Andrew West for his help and advice with the SDSS data.

## REFERENCES

Babul A., Rees M.J., 1992, MNRAS, 255, 346
Bertin E., Arnouts A., 1996, A&A, 117, 393
Binggeli B., Sandage A., Tarenghi M., 1984, AJ, 89, 64
Blanton et al., 2001, AJ, 121, 2358
Bradac M., Schneider P., Steinmetz M., Lombardi M., King L. J., Porcas R., 2002, A&A, 388, 373
Bullock J. S., Kravtsov A. V., Weinberg D. H., 2000, ApJ, 539, 2
Chiboucas K., Mateo M., 2001, Bull. Am. Astron. Soc., 33, 1459
Cole S., Lacey C. G., Baugh C. M., Frenk C. S., 2000, MNRAS, 319, 168
Conselice C. J., Gallagher J. S. III, Wyse R. F. G., 2001, ApJ, 559, 791
Cross N. J. G., Driver S. P., 2002, MNRAS, 329, 579
Cross et al., 2001, MNRAS, 324, 825
Cross N. J. G., Driver S. P., Liske J., Lemon D. J., Peacock J. A., Cole S., Norberg P., Sutherland W. J., 2004, MNRAS, 349, 576
Dalal N., Kochanek C. S., 2002, ApJ, 572, 25
Deady J. H., Boyce P. J., Phillipps S., Drinkwater M. J., Karick A., Jones J. B., Gregg M. D., Smith R. M., 2002, MNRAS, 336, 851
Dekel A., Silk J., 1986, ApJ, 303, 39



Downloaded from https://academic.oup.com/mnras/article/352/2/478/1011536 by guest on 23 February 2023

de Vaucouleurs 1961, ApJS, 6, 213
Dijkstra M., Haiman Z., Rees M., Weinberg D., 2004, ApJ, 601, 666
Driver S. P., 1999, ApJ, 526, L69
Driver S. P., de Propis R., 2003, Ap&SS, 285, 175
Efstathiou G., 1992, MNRAS, 256, 43P
Ferguson H., Binggeli B., 1994, A&AR, 6, 67
Font A. S., Navarro J. F., Stadel J., Quinn T., 2001, ApJ, 563, L1
Jerjen H., Rekola R., Takalo L., Coleman M., Valtonen M., 2001, A&A, 380, 90
Jerjen H., Binggeli B., Barazza F., 2004, AJ, 127, 771
Kambas A., Davies J. I., Smith R. M., Bianchi S., Haynes J. A., 2000, AJ, 120, 3
Kamionkowski M., Liddle A. R., 2000, Phys. Rev. Lett., 84, 4525
Kauffmann G., White S. D. M., Guideroni B., 1993, MNRAS, 264, 201
Klypin A., Kravtsov A. V., Valenzuela O., Prada 1999, ApJ, 522, 82
Kochanek C. S., Dalal N., 2003, in AIP Conf. Proc. Vol. 666. The Emergence of Cosmic Structure: 13th Astrophysics Conference. Am. Inst. Phys., New York, p. 103
Kogut A. et al., 2003, ApJS, 148, 161
Liske J., Lemon D. J., Driver S. P., Cross N. J. G., Couch W. J., 2003, MNRAS, 344, 307
Lemson G., Kauffmann G., 1999, MNRAS, 302, 111
Mateo M., 1998, ARA&A, 36, 435
Mathis H., Lemson G., Springel V., Kauffmann G., White S. D. M., Eldar A., Dekel A., 2002, MNRAS, 333, 739
Metcalf R. B., Zhao H., 2002, ApJ, 567, L5
Milne M. L., Pritchet C. J., 2002, A&AS, 201, 4211
Moore B., Lake G., Quinn T., Stadel J., 1999a, MNRAS, 304, 465
Moore B., Ghigna S., Governato F., Lake G., Quinn T., Stadel J., 1999b, ApJ, 524, L19
Norberg P. et al., 2002, MNRAS, 336, 907
Phillipps S., Parker Q., A., Schwartzenberg J. M., Jones J. B., 1998, ApJ, 493, L59
Pritchet C., van den Bergh S., 1999, AJ, 118, 883
Sabatini S., 2003, PhD thesis, University of Cardiff
Sabatini S., Scaramella R., Testa V., Andreon S., Longo G., Djorgovsky G., De Carvalho R. R., 1999, Mem. Soc. Astron. Ital., 71, 1091
Sabatini S., Davies J., Scaramella R., Smith R., Baes M., Linder S. M., Roberts S., Testa V., 2003, MNRAS, 341, 981
Sabatini S. et al., 2004, MNRAS, submitted
Tóth G., Ostriker J. P., 1992, ApJ, 389, 5
Trentham N., 1997, MNRAS, 286, 133
Trentham N., Hodgkin S., 2002, MNRAS, 333, 423
Trentham N., Tully R. B., 2002, MNRAS, 335, 712
Trentham N., Tully R. B., Verheijen M. A. W., 2001, MNRAS, 325, 385
Tully R. B., Somerville R. S., Trentham N., Verheijen M. A. W., 2002, ApJ, 569, 573
Valotto C., Moore B., Lambas D., 2001, ApJ, 546, 157
Velázquez H., White S. D. M., 1999, MNRAS, 304, 254
Young A., Wilson A., Mundell C., 2002, ApJ, 579, 560

This paper has been typeset from a TEX/LATEX file prepared by the author.

Downloaded from https://academic.oup.com/mnras/article/352/2/478/1011536 by guest on 23 February 2023